CrystEngComm

Vapour-liquid-solid-like growth of high-quality and uniform 3C-SiC heteroepitaxial films on α-Al_2O_3(0001) substrates

Journal:	*CrystEngComm*
Manuscript ID	CE-ART-12-2020-001793.R1
Article Type:	Paper
Date Submitted by the Author:	09-Jan-2021
Complete List of Authors:	Sannodo, Naoki; Tohoku University, Engeneering Osumi, Asuka; Tohoku University, Engeneering Kaminaga, Kenichi; Tohoku University, Engeneering Maruyama, Shingo; Tohoku University, Applied Chemistry Matsumoto, Y.; Tohoku Univ,

ARTICLE

Vapour-liquid-solid-like growth of high-quality and uniform 3C-SiC heteroepitaxial films on α-Al_2O_3(0001) substrates

Received 00th January 20xx,
Accepted 00th January 20xx

DOI: 10.1039/x0xx00000x

Naoki Sannodo, [a] Asuka Osumi, [a] Kenichi Kaminaga, [a] Shingo Maruyama[a] and Yuji Matsumoto*[a]

We demonstrate a heteroepitaxial growth of 3C-SiC thin films on α-Al_2O_3(0001) substrates by a vapour-liquid-solid (VLS)-like mechanism, an advanced process of alternating deposition of SiC and $NiSi_2$ flux in nanoscale, which process is facilitated by our pulsed laser deposition system with rapid beam deflection (RBD-PLD). In the VLS-like growth, different from conventional VLS processes, the nanoscale liquid precursors diffuse over the substrate and are highly and uniformly dispersed, preventing possible effects on the substrate etching and subsequent film growth by locally aggregated flux. As a result, the VLS-like growth process is found to work effectively even in heteroepitaxial growth of uniform and high-quality SiC films with a low inclusion of carbon impurity, as evidenced by X-ray diffraction, scanning electron microscopy, Raman spectroscopy and UV-vis spectroscopy. These results illustrate the versatility of the VLS-like growth process for uniform and high-quality crystal thin films of various materials in heteroepitaxial systems.

Introduction

Silicon carbide (SiC) has attracted much attention as one of the next-generation semiconductor materials because of its superior properties compared with the existing semiconductors such as Si, GaAs and InP. SiC has numerous polytypes defined by the stacking sequence of the Si-C bilayer along the direction normal to the close packed plane. Among the polytypes, 4H- and 3C-SiC are the most popularly known for their characteristics, particularly technological important in industrial applications. That is, 4H-SiC, which has a wide bandgap of 3.26 eV, a high breakdown electric field strength, a high-saturated drift velocity, and high thermal stability,[1-3] is a promising material for the use in efficient and lightweight power devices for high-frequency and high-temperature operation.[4-6] On the other hand, 3C-SiC, which is the only cubic polytype with no crystallographic anisotropy, has high electron mobility and shows excellent metal-oxide-semiconductor (MOS) properties; it is expected to be used as field-effect transistors and capacitors based on the MOS structure.[7-11] Furthermore, 3C-SiC is chemically stable and has a narrower bandgap of 2.23 eV[12] than 4H-SiC, capable of absorbing a large part of solar light, making it a promising visible-light photocatalyst. Nowadays, there have been some attempts of 3C-SiC to be used in nanoparticle or thin film form as photocatalysts for water splitting and CO_2 reduction in aqueous solution.[13-18]

As mentioned above, SiC polytypes have different applications, respectively, depending on their crystal structures and properties; it is hence necessary to develop process techniques for the selective growth of each SiC polytype. 4H-SiC bulk crystals for wafer use have been commonly produced by a sublimation method at process temperatures above 2000°C.[19] In contrast, the sublimation method would not be suitable for the growth of 3C-SiC bulk crystals because the 3C polytype does not favour such high process temperatures in terms of its thermodynamic stability.[20] Therefore, the growth of most 3C-SiC crystals has been attempted in epitaxial film form through vapour deposition processes such as chemical vapour deposition (CVD)[21] and pulsed laser deposition (PLD).[22] However, the crystal quality of these 3C-SiC films is not satisfactory because it would be difficult to achieve uniform and large grains at any process temperatures low enough to selectively grow the 3C-SiC polytype in such non-equilibrium vapour deposition processes.

Recently, even in the growth of 4H-SiC bulk crystals, a flux growth method, which is one of the solution growth techniques, has received a growing interest as an alternative to the sublimation method. In principle, the flux growth method can produce high-quality 4H-SiC crystals for its relatively low growth temperatures, compared to the sublimation process, because the crystal growth proceeds nearly in the thermodynamic equilibrium condition through Si-based liquid flux.[23] In order to improve not only the crystal quality, but also the polytype selectivity and crystal growth rate, the various kinds of Si-based binary flux of Si-X in the growth of SiC bulk crystals have been so far reported for X = Fe,[24, 25] Ge,[26] Al,[27] Ni[28] and Cr[29]. Furthermore, there also have been studied some kinds of Si-based ternary flux consisting of Si and two additive metals.[27, 30]

In these backgrounds, it is a vapour-liquid-solid (VLS) mechanism that has attempted to introduce such flux-like effects into vapour deposition processes for SiC films. Because of its potential of lowering the process temperature compatible

[a] Department of Applied Chemistry, Tohoku University, Sendai, 980-8579, Japan. E-mail: y-matsumoto@tohoku.ac.jp

†Electronic Supplementary Information (ESI) available: [details of any supplementary information available should be included here]. See DOI: 10.1039/x0xx00000x

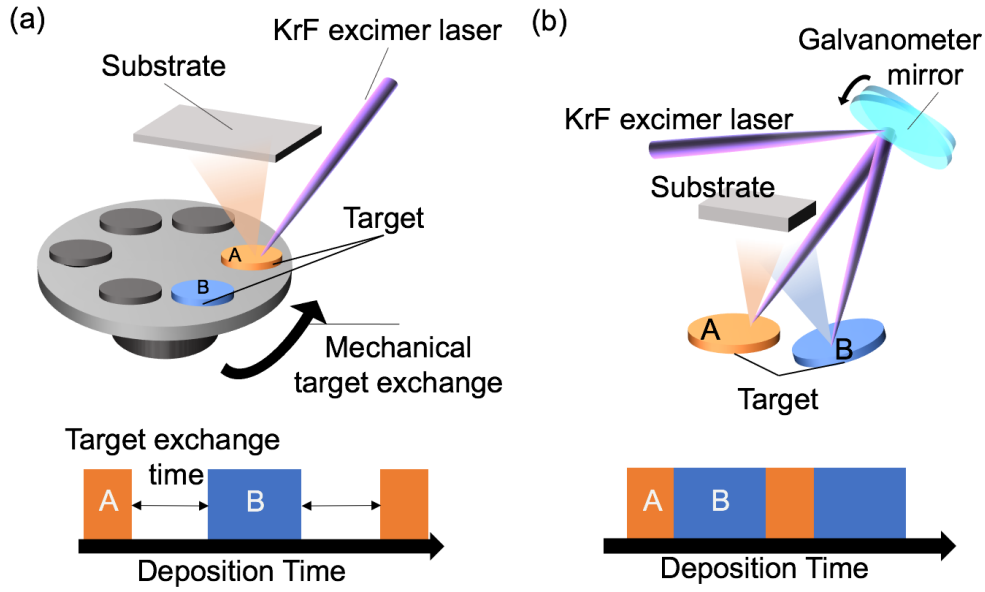

Fig. 1 Schematic of two types of PLD systems: (a) mechanical target exchange-type conventional PLD and (b) PLD system with rapid beam deflection by galvanometer mirror, together with a typical time chart during deposition of two targets in each PLD system.

with high crystallinity even in vapour deposition, there have been many reports on the homoepitaxial VLS growth of not only 4H- but also 3C-SiC films, in most of which 6H- or 4H-SiC single crystal substrates are used.[31, 32] For further investigation of fundamental properties of SiC films and development of unique functionalities of their devices, it would be also required to establish heteroepitaxial VLS growth techniques for each different polytype, especially for the 3C-polytype.[7, 8] The purpose of the present study is therefore to grow 3C-SiC films on α-Al_2O_3 single crystal substrates by using $NiSi_2$ liquid flux, which was found to be effective for the homoepitaxial VLS growth of 3C-SiC films in our previous study.[33] Unfortunately, however, the conventional VLS processes using bulky flux would not be available for such a heteroepitaxial growth of SiC films because of a possible, unfavoured substrate etching by the bulky flux. If it is even at the initial stage of the VLS process, the growth interface may become rough, hence inhibiting the uniform growth of SiC films, or some of the atoms dissolved out of the substrate could be incorporated into the growing films, leading to their unsatisfactory characteristics. For example, it has been reported that uniform SiC films on α-Al_2O_3 or Si substrates can be fabricated by deposition processes without using any liquid flux,[34-36] whereas in a heteroepitaxy of SiC films on a Si substrate by the VLS process, some cavities were reportedly formed at the film/substrate interface, or no single-oriented films were obtained because of severe dissolution of the substrate surface.[37, 38] Furthermore, according to our preliminary investigation (Fig. S1), it was found that even a 10 nm-thick $NiSi_2$ flux pre-deposited on an α-Al_2O_3 single crystal substrate was ready to significantly etch the substrate at a temperature of 1000°C, forming many, more than 10-nm deep holes, because of dewetting and aggregation of the $NiSi_2$ flux on the α-Al_2O_3 substrate surface, different from the case on a SiC substrate surface.[39]

In order to avoid these potential problems in VLS growth for high-quality crystal films, we propose a VLS-like growth approach by PLD,[40] where a bulky flux source is not pre-prepared on a substrate, but a small part of the flux is intermittently supplied in every growth of the unit cell layer or less thick film. In fact, by using this VLS-like growth technique, we have succeeded in the homoepitaxial growth of high-quality 3C-SiC films without pre-deposition of bulky flux.[40] As the liquid flux precursors supplied by PLD in this process diffuse across the heated substrate surface and will not instantly aggregate into precipitates, there would be little chance of such deep substrate etching by the flux. In fact, the preliminary investigation also showed no significant etching of the substrate in the VLS-like model process (Fig. S1). Highly encouraged by this preliminary result, in this study, we attempt the heteroepitaxial growth of 3C-SiC films on α-Al_2O_3 substrates by the VLS-like growth approach and compare their growth behaviour and the resultant crystal quality with those of SiC films grown by the conventional VLS as well as by just PLD.

Experimental

Thin film fabrication

We used single-crystal α-Al_2O_3 (0001) wafers cut to 5 mm × 5 mm pieces as substrates for SiC heteroepitaxial growth. After ultrasonically cleaned with acetone, ethanol and ultrapure water, respectively, the α-Al_2O_3 substrate was mounted on a carbon plate (7 × 7 × 1 mm^3) with carbon paste. $NiSi_2$ was selected as a liquid flux for VLS-like and VLS growth of SiC films because it is easy to handle as it melts below 1000°C[41] and its carbon solubility is relatively high.[42]

Realization of the VLS-like growth requires a PLD system that can supply two components alternately at high speed. There

Table 1 Growth conditions of the samples.

Sample	Process	Deposition thickness at 1 cycle		Total amount		Number of cycle	Total deposition time
		SiC	$NiSi_2$	SiC	$NiSi_2$		
#1	PLD	-	-	200 nm	-	-	27 min
#2		0.1 nm/cycle	0.005 nm/cycle	200 nm	10 nm	2000	27 min
#3		0.1 nm/cycle	0.010 nm/cycle	200 nm	20 nm	2000	27 min
#4		0.1 nm/cycle	0.015 nm/cycle	200 nm	30 nm	2000	27 min
#5	VLS-like	0.1 nm/cycle	0.020 nm/cycle	200 nm	40 nm	2000	27 min
#6		0.1 nm/cycle	0.030nm/cycle	200 nm	60 nm	2000	27 min
#7		0.1 nm/cycle	0.040nm/cycle	200 nm	80 nm	2000	27 min
#8		0.1 nm/cycle	0.050 nm/cycle	200 nm	100 nm	2000	27 min
#9		-	-	200 nm	10 nm	-	27 min
#10		-	-	200 nm	20 nm	-	27 min
#11		-	-	200 nm	30 nm	-	27 min
#12	VLS	-	-	200 nm	40 nm	-	27 min
#13		-	-	200 nm	60 nm	-	27 min
#14		-	-	200 nm	80 nm	-	27 min
#15		-	-	200 nm	100 nm	-	27 min
#16	PLD	-	-	50 nm	-	-	6.75 min
#17	VLS-like	0.1 nm/cycle	0.015 nm/cycle	50 nm	7.5 nm	500	6.75 min
#18	VLS	-	-	50 nm	2.5 nm	-	6.75 min

have been reported several such advanced PLD systems,[43-45] and we have developed a PLD system with rapid beam deflection (RBD-PLD: < 10-8 Torr).[46] Fig. 1 shows a schematic of two types of PLD systems: The conventional PLD system often requires the time to switch the target position mechanically, whereas the RBD-PLD system enables a fast alternating, quasi-simultaneous deposition of different target materials by scanning the laser beam between the positionally fixed targets with a galvanometer mirror without wait time.[42] In the present alternating deposition process, a substrate was first heated up to 1000°C by irradiating a continuous-wave infrared (IR) laser (λ = 808 nm) with a spot diameter of 5 mm from the backside of the carbon plate. Subsequently, SiC (3N in purity) and $NiSi_2$ (3N in purity) targets were alternately ablated with a KrF excimer laser (λ = 248 nm) to deposit SiC and liquid flux sources onto the substrate. The duration time per pulse was 25 ns, the focal spot size was 0.087 cm^2 and the distance between the targets and the substrate was set to 50 mm. For estimating the deposition rate of both targets (nm/pulse) in advance, we deposited each target material on a glass substrate with a total pulse number of 20000. After the deposition, we measured the thickness by a surface profiler (Surfcoder ET 4000A, Kosaka Lab. Ltd.) and calculated the deposition rate for each. Alternating deposition of 0.1 nm SiC and an arbitrary amount of $NiSi_2$ was defined as one cycle and repeated for 2000 cycles (i.e. the total thickness of SiC amounted to 200 nm). The thickness of $NiSi_2$ deposited per cycle was varied between 0 nm and 0.05 nm (the corresponding total volume ratio to the SiC film was ranged from 0 to 50 vol%). On the other hand, in the VLS growth process, an arbitrary thick $NiSi_2$ flux layer was first deposited onto a substrate at room temperature, and then the substrate was heated up to 1000 ˚C to melt the $NiSi_2$ flux layer. After that, a 200 nm thick SiC film was deposited on the flux-covered substrate at the temperature of 1000 ˚C. Deposition conditions for all the samples are summarized in Table 1(#1~#15). Since the total deposition times are all set to 27 minutes regardless of the film fabrication conditions, the effect that the surface annealing has on the growth process could be exactly the same between the samples and neglected in discussing the results. After deposition, all the samples were wet-etched with an $HF:HNO_3$ (1:1) solution to eliminate the residual solidified Ni-Si flux on the SiC film surface.

Thin film characterization

The surface morphology of SiC films was observed using scanning electron microscopy (SEM, S-4800, Hitachi, Ltd.) and atomic force microscopy (AFM, SP400, Seiko Instrument). Flatness and surface cleanness of the fabricated films were examined by reflection high energy electron diffraction (RHEED, Pascal Co., Ltd.). Raman spectroscopy (NRS-5100, JASCO, Ltd.) was used to identify the excess carbon inclusion in SiC films. The orientation, epitaxial relationship and crystallinity of SiC films were characterized by X-ray diffractometer (XRD, Bruker, D8 DISCOVER) through XRD 2θ scan, ϕ-scan and rocking curve measurements, respectively.

The optical absorption property of SiC films was investigated through UV-vis spectroscopy (UV-vis, UV-2450, Shimadzu Corporation). From UV-vis transmittance and reflectance spectra, the optical absorption coefficient α was calculated by the following equation,

$$\alpha = -\frac{1}{d}\ln\frac{T}{1-R}\frac{1-R_s}{T_s}$$

, where d is the film thickness, and T and R are the transmittance and reflectance of the sample, and T_s and R_s are those of an α-Al_2O_3 substrate for reference. It is noted that we used 50 nm-thick SiC films instead of 200 nm-thick films in the UV-vis spectroscopy experiment to avoid the influence of an

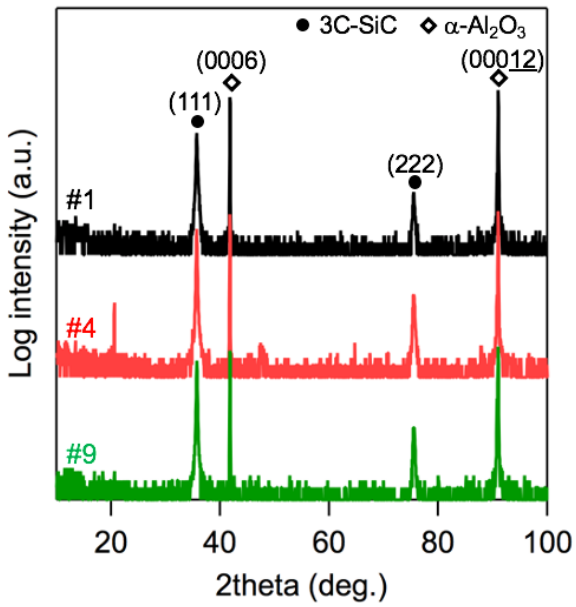

Fig. 2 Set of XRD 2θ patterns for the SiC film samples #1, #4 and #9 after wet-etching.

interference of light within the SiC film superimposed on the UV-vis spectra. The deposition conditions of the 50 nm-thick SiC films are also summarized in Table 1 (#16~#18).

Results and discussion

Fig. 2 shows a set of representative XRD 2θ patterns taken after wet-etching for the samples #1, #4 and #9, i.e., the SiC films fabricated by just PLD, VLS-like and VLS processes, respectively. For all these samples, we observe a pair of two diffraction peaks originating from crystal SiC around at 2θ = 35.6° and 75.5°, which peaks are attributable to 111 and 222 reflections of 3C-SiC. This is because, as will be discussed on the epitaxial relationship between the film and the substrate, the {220} reflections of 3C-SiC(111) are also observed in XRD ϕ-scan measurement, which can be detected when 3C-SiC(111) films grow. For the other samples with different amounts of $NiSi_2$, the 111 and 222 reflections of 3C-SiC are also observed in their XRD 2θ patterns. From these results, we therefore confirmed that 3C-SiC(111) crystal films grew on α-Al_2O_3(0001) substrates, regardless of the process and the flux amount. Cross-sectional SEM images of SiC films also showed that 200 nm SiC grew under all the present deposition conditions (Fig. S2). In the VLS growth with large amounts of $NiSi_2$ e.g., for the sample #12, some diffraction peaks assigned to Ni-Si alloy crystals are detected around at 2θ of 40˚ to 50 ° in the XRD pattern taken before the wet-etching (Fig. S3(a), black line). The appearance of these alloy peaks suggests a possible formation of some bulk-sized flux precipitates through the aggregation of $NiSi_2$ in the VLS process; their presence was, as expected, confirmed by SEM observation of the VLS-grown sample before the wet-etching (the upper panel of Fig. S3(b)). In fact, the alloy peaks almost disappeared and was found the traces of precipitates on the surface after the wet-etching (Fig. S3(a), red line and the lower panel of Fig. S3(b)); we therefore conclude that most $NiSi_2$ was self-segregated and precipitated onto the film surface rather than included in the film during the growth. In contrast, no Ni-Si alloy peaks are observed in the XRD 2θ patterns before nor after the wet-etching in any of the films fabricated by the VLS-like process, the reason for which is probably the better wettability of liquid Si on SiC than Al_2O_3,[39] as already pointed out. During the early stage of the VLS-like process, the first deposited SiC may form a SiC seed layer all over the substrate, and thus the following supplied $NiSi_2$ precursors are well dispersed to uniformly cover the entire seed surface. In the VLS process, however, the bulky amount of $NiSi_2$ that was first deposited directly on the substrate may be locally aggregated on the surface, as inferred by the result of Fig. S1.

In Fig. 3 (a) and (b), the XRD peak intensity of 3C-SiC (111) that normalized by that of α-Al_2O_3(0006) and its rocking curve FWHM value, which were both measured after wet-etching, are plotted as a function of the amount of $NiSi_2$ (nm), respectively. From these plots, the addition of $NiSi_2$ is, on the one hand, clearly found to improve the crystallinity of the SiC films,

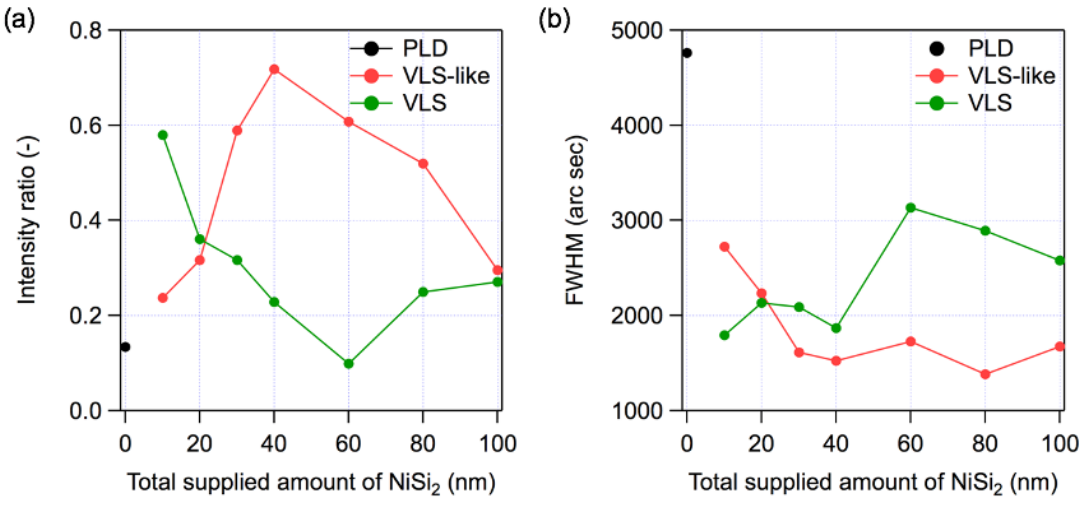

Fig. 3 XRD peak intensity of 3C-SiC (111) normalized by that of α-Al_2O_3(0006) and its rocking curve FWHM value, which were both measured after wet-etching, plotted as a function of the amount of $NiSi_2$ (nm), respectively.

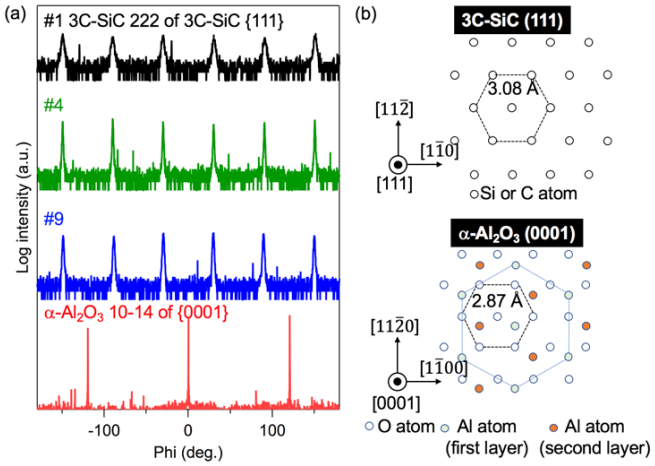

Fig. 4 (a) ϕ-scan diffraction patterns for the 3C-SiC 220 reflections of 3C-SiC {111} and α-Al_2O_3 10-14 reflections of α-Al_2O_3 {0001} for the samples #1, #4 and #9. Their in-plane epitaxial relationships between the substrate and SiC films are identical regardless of the fabrication process. (b) Schematic illustration of the in-plane epitaxial relationship between the 3C-SiC (111) film and the α-Al_2O_3(0001) substrate.

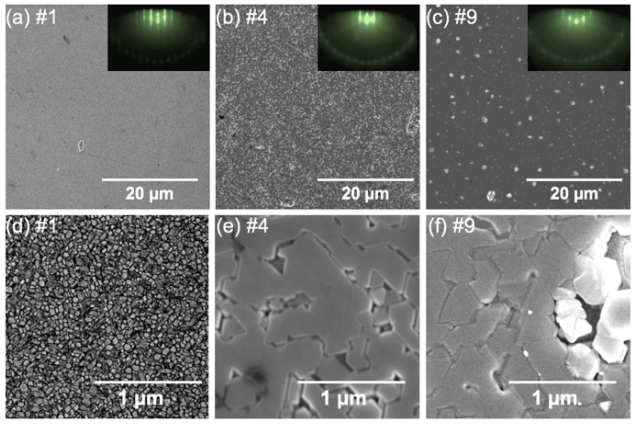

Fig. 5 SEM images for the samples #1, #4 and #9 at low and high magnification. Insets in (a), (b) and (c) are RHEED patterns taken along the [1-100] azimuth on the SiC film surfaces after surface cleaning and removing the remaining $NiSi_2$ by wet-etching.

regardless of whether it is in VLS-like or VLS growth. On the other hand, the optimal amounts of $NiSi_2$ are different between the processes, e.g., 40 nm and 10 nm in the VLS-like and VLS processes, respectively, in terms of the XRD peak intensity ratio. Turning our attention to the rocking curve FWHM, it seems not much depending on the amount of $NiSi_2$ in the VLS-like process, almost constant to be the lowest value of around 1500 arcsec within the uncertainty for the amounts of $NiSi_2$ equal to or greater than 30 nm.

Fig. 4(a) shows ϕ-scan patterns of the {220} reflections of 3C-SiC from the film samples #1, #4 and #9 as well as the corresponding ϕ-scan pattern of the {10-14} reflections of an α-Al_2O_3 substrate for comparison. The three {10-14} diffraction peaks in the ϕ-scan appear every 120 degrees, reflecting the trigonal symmetry of α-Al_2O_3. On the other hand, the 3C-SiC {220} diffraction peaks in the ϕ-scan appear every 60 degrees, seemingly with a six-fold symmetry, regardless of the fabrication process. The observed six-fold symmetry indicates that the 3C-SiC (111) films heteroepitaxially grow on α-Al_2O_3 (0001) with twin domains called double-positioning boundaries (DPBs),[48] which twin domains are rotated relative to each other around the [111] axis by 60 degrees. Such a double domain orientation has been commonly found in several heteroepitaxial systems of cubic-lattice structure films on α-Al_2O_3 (0001) substrates.[49, 50] The 3C-SiC {220} and α-Al_2O_3 {10-14} peaks are separated by 30 degrees; it follows that the epitaxial relationship has been determined to be 3C-SiC(111) [11-2]// α-Al_2O_3(0001) [11-20] (Fig. 4(b)), where the surface unit cell parameters of 3C-SiC (111) and the oxygen sublattice of α-Al_2O_3(0001) are 3.08 Å and 2.87 Å,[20, 51] respectively, with the in-plane lattice mismatching minimized as small as 7.3 %. There have been several reports that 3C-SiC films can epitaxially grow on Si and α-Al_2O_3 substrates by PLD also using an Nd:YAG laser at substrate temperatures around 1000˚C.[34, 52]

Fig. 5 shows a set of SEM images at low and high magnification, along with RHEED patterns (insets attached to the SEM images), for the SiC thin films after wet-etching. Just-PLD or VLS-like grown SiC films are uniform over a wide area (Fig. 5(a) and (b)), whereas the VLS-grown SiC film shows some white spots (Fig. 5(c)). In the VLS process, even a small amount of $NiSi_2$ may aggregate on the substrate to form bulky liquid precipitates, as more clearly found in Fig. S3(b). If this is the case, the VLS growth proceeds more effectively within the precipitates, and the resultant relatively bulky crystal grains are imaged as white spots in the SEM image; meanwhile, outside region of the precipitates, there are plain SiC grains grown as found in the VLS-like growth (Fig. 5(f)). On the other hand, unlike the different results of the low-magnification SEM images, the three SiC film samples all exhibit sharp streaky patterns similar to each other, indicating that their local surface flatness is high enough, regardless of the fabrication process. As for the crystalline sizes and shapes of SiC, in contrast to not so significant difference in the XRD results as shown in Fig. 2, the high-magnification SEM images revealed that a granular structure (grain size less than ~100 nm) was observed in the sample #1 fabricated by just PLD (Fig. 5(d)), while the crystalline sizes were much larger in the samples fabricated through VLS-like and VLS processes with $NiSi_2$ (Fig. 5(e)(f)) in comparison with those of SiC films fabricated by conventional PLD previously reported.[34, 52] This result suggests that $NiSi_2$ works as a liquid flux to a substantial extent like in bulk flux growth, probably promoting the diffusion of SiC precursors, irrespective of whether it is in the VLS-like or VLS process. However, there is found a specific difference in the crystal shape appearance of the obtained films between the VLS-like and VLS processes. There are various facets well developed in VLS-grown crystallites and deep trenches formed between the grains, as if these crystallites were nucleated and grown three-dimensionally in liquid, even outside regions of the precipitates, which situation is more significantly found when the $NiSi_2$ is more added (Fig. S4). On the other hand, there are relatively flat SiC crystallites densely packed on the film surface

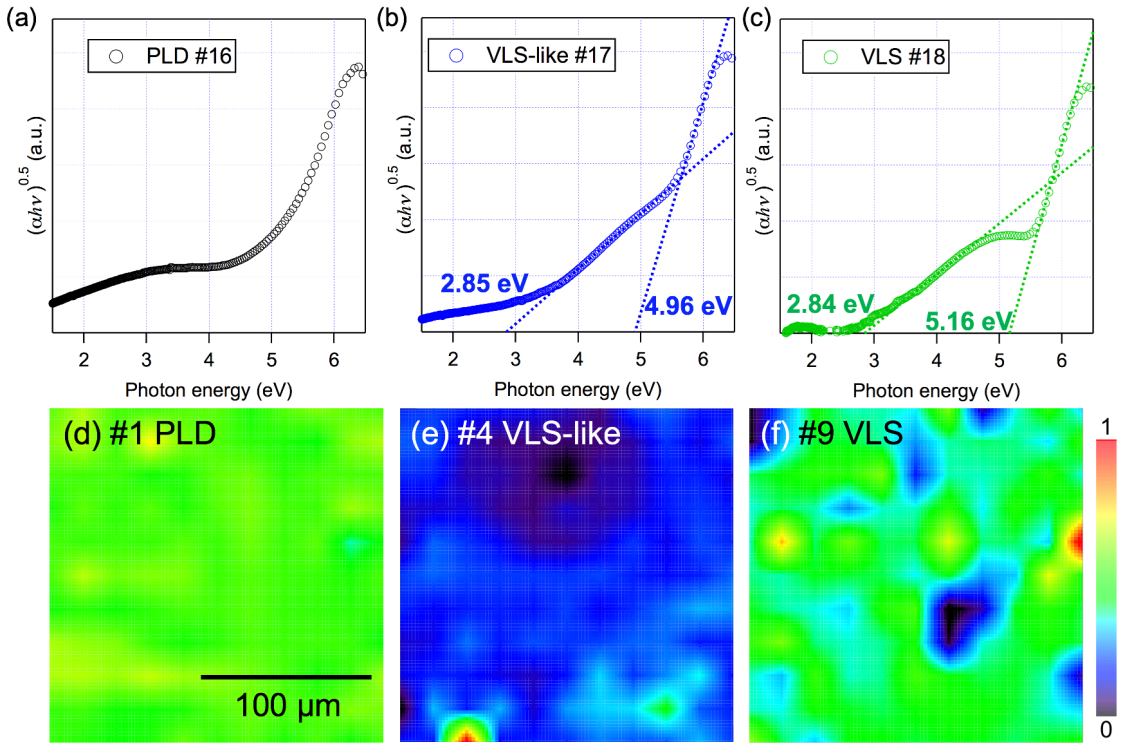

Fig. 6 (a)(b)(c) Tauc plots for indirect allowed transitions of the SiC films fabricated by PLD (#16), VLS-like growth (#17), and VLS growth (#18), respectively. (d)(e)(f) Set of Raman mapping images of the intensity ratio of the G-band of carbon (1600 cm^{-1}) and the A_{1g} peak of sapphire (418 cm^{-1})[48] in Raman spectra over the film region (200 μm * 200 μm) for the samples #1, #4 and #9.

in the VLS-like process. This suggests that even a small amount of $NiSi_2$ alternately supplied in each cycle rather promotes the two-dimensional in-plane growth of SiC crystallites, different from the VLS process. Indeed, in terms of the in-plane uniformity, the VLS-like grown films are acceptable comparable with the film fabricated by just PLD, while the VLS-grown films show some precipitates on the surface besides unavoidable inhomogeneous surface morphology, as typically observed in the SEM images of Fig. 5(c). Considering, thus, overall the SEM and XRD results depending on the amount of $NiSi_2$, the SiC film to give the best crystallinity is the sample #4 by the VLS-like process, whose optimal amount of $NiSi_2$ is likely to lie around 30 nm in thickness, while among the VLS-grown films the sample #9 is the best whose optimal amount of $NiSi_2$ is around 10 nm in thickness.

Based on the discussion above, 50 nm-thick SiC films corresponding to the samples of #4 and #9 as well as #1, that is, the optimized, best VLS-like and VLS grown films, and the just-PLD grown film, respectively, were fabricated for UV-vis absorption experiment (the samples #17, #18 and #16). Fig. 6(a), (b) and (c) show the absorption spectra of the 50 nm-thick SiC films, calculated from the UV-vis transmission and reflection spectra. There are two inflection points in each spectrum for the samples #17 and #18, yielding two indirect optical bandgaps, respectively. From the tauc plot analysis, the indirect bandgap was determined to be 2.9 eV in average, similar to the experimental values of the narrowest 3C-SiC indirect transition reported for SiC films fabricated by PLD, [53, 54] while the second indirect bandgap was to be 5.1 eV in average, which is close to be the theoretical value of the second narrowest indirect transition of the optical band gap of 3C-SiC.[55] However, these two bandgap values are slightly larger than the values of the stoichiometric 3C-SiC which are predicted from the theoretical calculation. [55] These results suggest that a sizable deficiency of Si atoms in the SiC lattice led to the widening of the optical bandgap of SiC films.[56] On the other hand the single bandgap estimated from the tauc plot for the sample #16 in Fig. 6(a), is smaller than those of the samples #17 and #18, which might be due to not-negligible amounts of defects and impurities included in the PLD-grown film. It should be noted that the three 50 nm thick samples #16, #17, and #18 used in the UV-vis measurement were different from the corresponding 200 nm thick samples #1, #4, and #9 in their surface morphology and grain sizes (Fig. S5). In particular, the grain sizes of the VLS-like grown sample #17 were larger than those of the PLD-grown sample #16, but seemingly not so much improved as compared to the case of the thick films. Nevertheless, there was still found a significant difference in their optical absorption property. This result suggests that, as discussed above, the optical absorption property such as the bandgap is influenced mainly by the composition of Si and C and the presence of defects, but not so much by the grain sizes of SiC.

In terms of the uniformity of SiC films, we examined the spatial distribution of carbon aggregates by mapping the intensity ratio of the G-band of carbon (1600 cm^{-1}) / the A_{1g} peak of sapphire (428 cm^{-1})[57] in Raman spectra over the film region (200 μm x 200μm) for the samples #1, #4 and #9, as shown in Fig. 6(d), (e) and (f), respectively. In the just-PLD grown film (Fig. 6(d)), the intensity ratio was higher than 0.5 all over the region but showed small spatial dependence, indicating almost the uniform presence of carbon aggregates in the entire film. In general, Si atoms can evaporate during the deposition of SiC

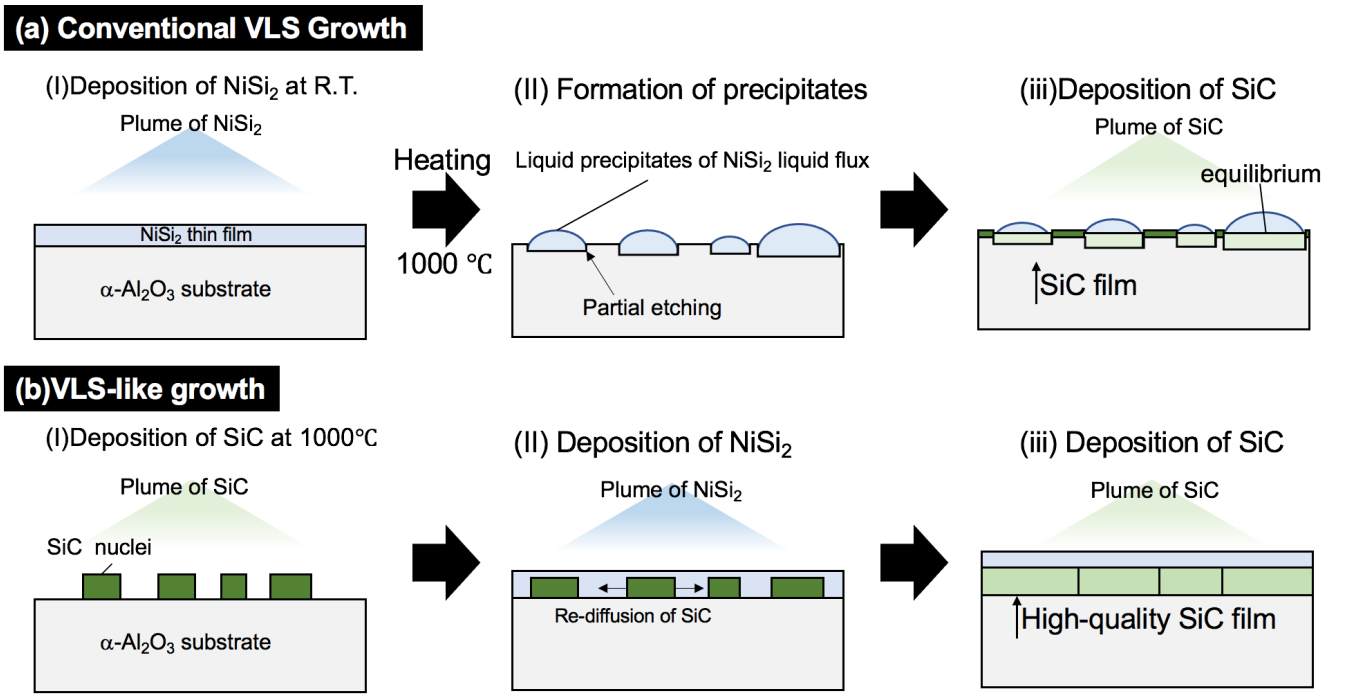

Fig. 7 Schematic illustration of the growth mechanism of SiC films by the conventional VLS (a) and by VLS-like growth (b).

films at high temperatures under a vacuum, e.g., in the present PLD conditions of 1000°C and 10^{-7} Torr,[58] leaving the excess carbon atoms on the growing film surface to form such carbon clusters. On the other hand, the VLS-grown SiC film show relatively high-intensity ratios in most film regions, although there are found some spot regions with much lower-intensity ratios (Fig. 6(f)). The existence of these low-intensity spot regions is another evidence that even a small amount of $NiSi_2$ forms liquid precipitates and the VLS growth of SiC proceed effectively within them to result in SiC crystals with almost no inclusion of carbon aggregates as discussed in Fig. 5. In contrast, the intensity ratios of the VLS-like grown SiC film are much lower over the entire film region as shown in Fig. 6(e). It is therefore considered that $NiSi_2$ precursors, which is diffusible and uniformly dispersed over the entire substrate, may cover the SiC film surface to kinetically suppress the volatilization of Si atoms like a surfactant and/or be a source of additional Si atoms that compensate for the Si deficiency in the SiC film.

Finally, for comparison, Fig. 7 shows a schematic illustration of crystal growth models of the conventional VLS and VLS-like processes, respectively. In the conventional VLS growth process, a pre-deposited $NiSi_2$ film first melts and forms liquid precipitates when the substrate temperature reaches the melting point of $NiSi_2$, and it is then followed by the supply of Si and C precursors. In this case, the three-dimensional-like liquid phase growth proceeds effectively within the precipitates. On the other hand, in the VLS-like process, SiC firstly nucleates and forms a sort of a buffer layer for the subsequently deposited $NiSi_2$ precursors so that they diffuse and are highly and uniformly dispersed over the SiC buffer layer because of a relatively high wettability of $NiSi_2$ to SiC surfaces. Such $NiSi_2$ mobile precursors can still collectively work to have a flux-like effect to promote the crystal growth of SiC, though too much added $NiSi_2$ may act as bulky flux causing the results like in the conventional VLS process. The existence of such $NiSi_2$ mobile precursors is also suggested even in the VLS process, focusing on the outside region of precipitates. In fact, there are found plain and relatively large SiC grains like those in the VLS-like growth. This suggests that not all of the deposited $NiSi_2$ are aggregated to form such precipitates, and the residual, not-negligible amount of $NiSi_2$ mobile precursors should still work to have a similar flux-like effect. In any cases, such a flux-like effect to promote the crystal growth would rely on some molecular or atomic level chemical interactions by the growing SiC being exposed to such $NiSi_2$ mobile precursors.

Conclusions

We have demonstrated the heteroepitaxial growth of 3C-SiC films on α-Al_2O_3 (0001) substrates through the VLS-like process using $NiSi_2$ as a flux. $NiSi_2$ supplied to the heated substrate surface was uniformly diffused and dispersed, and even a small amount of $NiSi_2$ was found enough to cause a flux-like effect. The advantage of the VLS-like growth in the heteroepitaxial growth is to enable to prevent partial etching of the substrate by liquid precipitates, improving the uniformity of high-quality 3C-SiC films under quasi-thermodynamically equilibrium conditions. VLS-like growth is hence a promising approach to achieve uniform and high-quality heteroepitaxial films of various materials.

Conflicts of interest

There are no conflicts to declare.

Acknowledgements

This work was supported by the Advanced Low Carbon Technology Research and Development Program (ALCA) of the Japan Science and Technology Agency (JST).

Notes and references

1 L. Patrick, W. J. Choyke and D. R. Hamilton, *Phys. Rev.*,1965, **137**, A1515-A1520.
2 A. O. Konstantinov, Q. Wahab, N. Nordell and U. Lindefelt, *J. Electron. Mater.*, 1998, **27**, 335-341.
3 R. Mickevicius and J. H. Zhao, *J. Appl. Phys.*, 1998, **83**, 3161-3167.
4 G. Muller, G. Krotz, E. Niemann, *Sens. Actuat. A Phys.*, 1994, **43**, 259-268.
5 D.M. Brown, E. Downey, M. Grezzo, J. Kretchmer, V. Krishnamethy, W. Hennessy and G. Michon, *Solid State Electron*, 1996, **59**, 1531-1542.
6 S. Mounce, B. McPherson, R. Schupbach, and A. B. Lostetter, *Proc. IEEE Aerosp. Conf.*, 2006, 1–19.
7 R. Oka, K. Yamamoto, H. Akamine, D. wang, H. Nakashima, S. Hishiki and K. Kawamura, *Jpn. J. Appl. Phys.*, 2020, **59**, SGGD17.
8 R. Anzalone, S. Privitera, M. Camarda, A. Alberti, G. Mannino, P. Fiorenza, S. Di Franco and F. La Via, *Materials Science and Engineering B*, 2015, **198**, 14–19.
9 M. Kobayashi, H. Uchida, A. Minami, T. Sakata, R. Esteve and A. Schoner, *Mater. Sci. Forum*, 2011, **679**, 645-648.
10 K. Cherkaoui, A. Blake, Y. Y. Gomeniuk, J. Lin, B. Sheehan, M. White, P. K. Hurley and P. J. Ward, *AIP Advances*, 2018, **8**, 085323.
11 J. Wan, M.A. Capano, M. R. Melloch and J. A. Cooper, *IEEE Electron Device Letters*, 2002, **23**, 482-484.
12 G. L. Zhao and D. Bagayoko, *New J. Phys.*, 2000, **2**, 16.
13 T. Yasuda, M. Kato and M. Ichimura, *Mater. Sci. Forum*, 2012, **717**, 585-588.
14 H. Li, Y. Lei, Y. Huang, Y. Fang, Y. Xu, L. Zhu and X. Li, *J. Nat. Gas Chem.*, 2011, **20**, 145-150.
15 M. Aslam, M. T. Qamar, I. Ahmed, · A. U. Rehman, S. Ali, I. M. I. Ismail and A. Hameed, *Applied Nanoscience*, 2018, **8**, 987-999.
16 J. Jian, Y. Shi, M. Syvajarvi, R. Yakimova and J. Sun, *Sol. RRL*, 2020, **4**, 1900364.
17 J. Jian, Y. Shi, S. Ekeroth, J. Keraudy, M. Syvajarvi, R. Yakimova, U. Helmerssona and J. Sun, *J. Mater. Chem. A*, 2019, **7**, 4721-4728.
18 J. T. Song, T. Iwasaki and M. Hatano, *Jpn. J. Appl. Phys.,* 2015, **54**, 04DR05.
19 Y. M. Tairov and V. F. Tsvetkov, *J. Cryst. Growth*, 1978, **43**, 209–212.
20 H. Matsunami, *Diam. Relat. Mater.*, 1993, **2**, 1043-1050.
21 Q. Sun, M. Yang, J. Li, Q. Xu, R. Tu, Q. Li, S. Zhang, L. Zhang, T. Goto, H. Ohmori and M. Kosinova, *J Am Ceram Soc.*, 2019, **102**, 4480–4491.
22 G. Monaco, D. Garoli, M. Natali, M.G. Pelizzo and P. Nicolosi, *Appl Phys A*, 2011, **105**, 225-231.
23 D. Elwell and H. J. Scheel, Crystal Growth from High-Temperature Solutions (New York: Academic)
24 T. Yoshikawa, S. Kawanishi and T. Tanaka, *Jpn. J. Appl. Phys.*, 2010, **49**, 051302.
25 S. Kawanishi and T. Yoshikawa, *JOM*, 2018, **70**, 1239-1247.
26 O. Filip, V. Epelbaum, M. Bickermann and A. Winnacker, *J. Cryst. Growth*, 2004, **271**, 142-150.
27 N. Komatsu, T. Mitani, Y. Hayashi, T. Kato, S. Harada, T. Ujihara and H. Okumura, *J. Cryst. Growth*, 2017, **458**, 37–43.
28 Y. Yonezawa, M. Ryo, A. Takigawa and Y. Matsumoto, *Sci. Technol. Adv. Mater.*, 2011, **12**, 054209.
29 Y. Hayashi, T. Mitani, N. Komatsu, T. Kato and H. Okumura, *J. Cryst. Growth*, 2019, **523**, 125151.
30 K. Hyun, T. Taishi, K. Suzuki and K. Teshima, *Mater. Sci. Forum*, 2018, **924**, 43-46.
31 G. Ferro and C. Jacquier, *New. J. Chem.*, 2004, **28**, 889-896.
32 M. Soueidan, G. Ferro, O. Kim-Hak, F. Cauwet and B. Nsouli, *Crystal Growth & Design*, 2008, **8**, 1044-1050.
33 A. Onuma, S. Maruyama, T. Mitani, T. Kato H. Okumura and Y. Matsumoto, *CrystEngComm*, 2016, **18**, 143.
34 T. Kusumori, H. Muto and M. E. Brito, Appl. Phys. Lett., 84 (2004) 1272-1274.
35 S. A. Kukushkin and A. V. Osipov, *J. Phys. D: Appl. Phys.*, **47** (2014) 313001.
36 S.A. Kukushkin, A.V. Osipov, A.V. Redkov, A.S. Grashchenko, N.A.Feoktistov, S.D. Fedotov, V.N. Statsenko, E.M. Sokolov and S.P. Timoshenkov, *Rev. Adv. Mater. Sci.*, **57** (2018) 82-96.
37 S. Berckmans, L. Auvray, G. Ferro, F. Cauwet, V. Souliere, E. Collard and C. Brylinski, *J. Cryst. Growth*, 2012, **354**, 119–128.
38 Y. L. Liang, S. Z. Lu, H. Y. Lee, X. Qi and J. L. Huang, *Ceramics International*, 2015, **41**, 7640–7644.
39 J. G. Li and H. Hausner, *Materials Letters*, 1992, **14**, 329-332.
40 N. Sannodo, A. Osumi, S. Maruyama, Y. Matsumoto, *Applied Surface Science*, 2020, **530**, 147153.
41 *Binary Alloy Phase Diagrams*, ed. T. B. Massalski, et al., ASM International, Materials Park, Ohio, 2nd edn, 1998, vol. 1.
42 S. Maruyama, A. Onuma, K. Kurashige, T. Kato, H. Okamura and Y. Matsumoto, *ACS Comb. Sci.*, 2013, **15**, 287-290.
43 S. Zhang, Z. He, X. Ji, W. Lu, C. Wang, Q. Shen and L. Zhang, *J. Appl. Phys.*, **115** (2014) 154906.
44 S. Zhang, W. Lu, C. Wang, Q. Shen and L. Zhang, *Appl. Phys. Lett.*, **101** (2012) 141602.
45 J. Sakai, C. Autret-Lambert, T. Sauvage, B. Courtois, J. Wolfman and F. Gervais, *J. Cryst. Growth*, **380**, (2013) 106-110.
46 S. Maruyama, N. Sannodo, R. Harada, Y. Anada, R. Takahashi, M. Lippmaa and Y. Matsumoto, *Rev. Sci. Instrum.*, 2019, **90**, 093901.
47 J. G. Li and H. Hausner, *Materials Letters*, 1992, **14**, 329-332.
48 H. S. Kong, B. L. Jiang, J. T. Glass and G. A. Rozgonyi, *Journal of Applied Physics*, 1988, **63**, 2645-2650.
49 K. Uchida, K. Yoshida, D. Zhang, A. Koizumi and S. Nozaki, *AIP Advances*, 2012, **2**, 042154.
50 T. Ha, I. Park, K. I. Sim, H. Lee, J. -S. Bae, S. J. Kim, J. P. Kim, T.-T. Kim, J. H. Kim, J. I. Jang and S.-Y. Jeong, *APL Mater.*, 2019, **7**, 031115.
51 L. Qiao, H. Y. Xiao, W. J. Weber and M. D. Biegalski, *Applied Physics Letters*, 2014, **104**, 221602.
52 A. S. Gusev, S. M. Ryndya, A. V. Zenkevich, N. I. Kargin, D. V. Averyanov and M. M. Grekhov, *Modern Electronic Materials*, **1** (2015) 120–125.
53 E. Paneerselvam, V. K. L. Narayanan, N. J. Vasa, M. Higashihata, D. Nakamura, H. Ikenoue and M. S. R. Rao, *Journal of Electronic Materials*, **48** (2019) 3468–3478.
54 G. Monaco, D. Garoli, M. Natali, F. Romanato and P. Nicolosi, *Cryst. Res. Technol.*, **46** (2011) 784-788.
55 C. Persson and U. Lindefelt, *J. Appl. Phys.*, 1997, **82**, 5496-5508.
56 A. Trejo, M. Calvino and M. Cruz-irisson, *International Journal of Quantum Chemistry*, 2010, **110**, 2455-2462.
57 S. P. S. Porto and R. S. Krishnan, *J. Chem. Phys.*, 1967, **47**, 1009-1012.
58 Bedampfungs-technik Verfahren Einrichtungen Anwendungen, S. Schiller and U. Heisig, VEB Verlag Technik, Berlin, 1975.

